

# Non-linear response to electric field in extended Hubbard models

D. Nasr Esfahani,<sup>\*</sup> L. Covaci,<sup>†</sup> and F. M. Peeters<sup>‡</sup>

*Departement Fysica, Universiteit Antwerpen, Groenenborgerlaan 171, B-2020 Antwerpen, Belgium*

The electric-field response of a one-dimensional ring of interacting fermions, where the interactions are described by the extended Hubbard model, is investigated. By using an accurate real-time propagation scheme based on the Chebyshev expansion of the evolution operator, we uncover various non-linear regimes for a range of interaction parameters that allows modeling of metallic and insulating (either charge density wave or spin density wave insulators) rings. The metallic regime appears at the phase boundary between the two insulating phases and provides the opportunity to describe either weakly or strongly correlated metals. We find that the *fidelity susceptibility* of the ground state as a function of magnetic flux piercing the ring provides a very good measure of the short-time response. Even completely different interacting regimes behave in a similar manner at short time-scales as long as the fidelity susceptibility is the same. Depending on the strength of the electric field we find various types of responses: persistent currents in the insulating regime, dissipative regime or damped Bloch-like oscillations with varying frequencies or even irregular in nature. Furthermore, we also consider the dimerization of the ring and describe the response of a correlated band insulator. In this case the distribution of the energy levels is more clustered and the Bloch-like oscillations become even more irregular.

PACS numbers: 71.30.+h, 71.27.+a

## I. INTRODUCTION

The investigation of real time dynamics of a closed system consisting of interacting particles is important not only for the evaluation of experimentally relevant quantities, but also supplies reliable information about the general properties of the Hamiltonian as long as one measures an appropriate set of observables throughout the propagation process<sup>1</sup>. This is of interest especially when the dimension of the Hilbert space is very large and accessing the whole energy spectrum is not possible. There exist several approaches to face the problem of real time propagation of closed interacting systems. Among them are the numerically exact polynomial expansions<sup>2</sup> or the approximate Lanczos propagation method<sup>3</sup>, the state of art time dependent density matrix renormalization group(tDMRG)<sup>4</sup> and non-equilibrium dynamical mean field theory(nDMFT)<sup>5,6</sup>. The common thread for all these methods is that it is not necessary to access the whole spectrum in order to evaluate time dependent expectation values, hence this makes it feasible to investigate a large class of interacting systems. The special case of electric breakdown of 1D Mott insulators has been realized experimentally either with a strong electric field<sup>7,8</sup> or through photo-induced metal insulator transitions in pump probe experiments<sup>9,10</sup>. Further interest was recently triggered by the realization of fermionic optical lattice experiments, where the electric field effect on systems with designed interactions could be realized<sup>11-14</sup>.

There exist several theoretical investigations on the real time dynamics of the Hubbard Hamiltonian, part of which focused on real time quench dynamics<sup>15-19</sup>, real time studies based on the relaxation dynamics of specifically prepared excited states<sup>20</sup> as well as the effect of an external electric field<sup>5,21-27</sup>. The electric break down of a one-dimensional Mott insulator has been theoret-

ically investigated<sup>28,29</sup> and the analysis was based on a Landau-Zener(LZ)<sup>30,31</sup> mechanism, which showed an exponential decay of the probability of the initial ground-state as function of time in short time scales. The decay rate is a function of an exponential function with an exponent proportional to square of the charge gap of the system<sup>29</sup>, however this is not universal and the dependence of the exponent on the charge gap could deviate from quadratic type for specific cases<sup>32</sup>. We found there are situations in which the breakdown is not simultaneous with the overlap of ground-state with only the first excited state but also with higher energy states. This happens especially for insulating systems with larger charge gaps. This therefore makes inappropriate the use of a simple two level approximation and the LZ parameter as a basis for comparing different insulating systems. In order to alleviate these discrepancies of the two level approximation we employ the recently proposed *fidelity susceptibility*<sup>33</sup> as a measure for the change of basis-set as function external field. This quantity is unbiased and can be calculated numerically exact. Throughout this work we use it as a basis for comparing the response of different insulating systems to a constant electric field.

Beyond the short time-scale ground-state decay, a question that grasped the attention is how much does the electric field response at longer time scales depends on ground-state properties and/or interaction parameters. A notable phenomenon that definitely depends on longer time scales and is beyond the ground state decay mechanism based on the Landau-Zener(LZ) tunneling is the appearance of Bloch oscillations(BO). The existence of Bloch oscillations has already been proven experimentally in semiconductor super-lattices<sup>34-37</sup>. Furthermore, the damping of Bloch oscillations in a closed interacting system subjected to an uniform electric field has been described theoretically within the Falikov-Kimbal model<sup>5</sup>,

the one-dimensional Hubbard spin-less model<sup>38</sup>, where it is shown an integrable system shows current oscillations with frequencies smaller than the normal BO when subjected to uniform weak field, and in the one dimensional Holstein model<sup>39</sup>, where authors report the presence of an stationary state which carries a finite current. Furthermore BO oscillations in electric break down of a 3-dimensional Hubbard model<sup>24</sup> is investigated. By using an extended Hubbard model one has the opportunity to design the interaction parameters in order to have better understanding about the mechanism of the formations of BO in different regimes, and it is the aim of this paper to investigate the differences between the non-linear response of different kinds of closed systems of interacting fermions both in the insulating and the metallic regimes. We achieve this by employing a real time propagation scheme together with the ground-state and spectral analysis. Based on our analysis it appear to be impossible for a closed system to have an stationary state which carries finite stationary current. Our paper is organized as follows: in Sec. II we present our model under study together with a brief description of the theoretical and numerical schemes. In Sec. III(A) we present our analysis of the response to constant electric field for a system of weakly interacting fermions, while in Sec. III(B) we perform the same study but for strongly interacting fermions. Finally, in Sec. IV we give our conclusions.

## II. MODEL AND METHOD

Our model under investigation is a one-dimensional closed system of interacting charged fermions with periodic boundary conditions. It can be described in the second-quantization formalism by an extended Hubbard model as follows:

$$\hat{H} = - \sum_{\langle ij \rangle \sigma} [h_{ij}(t) \hat{c}_{i\sigma}^\dagger \hat{c}_{j\sigma} + h.c.] + \sum_{\langle ij \rangle} \frac{1}{2} V_{ij} \hat{n}_i \hat{n}_j + \sum_i U \hat{n}_{i\sigma} \hat{n}_{i\bar{\sigma}}, \quad (1)$$

where  $\langle \dots \rangle$  represents the summation over the nearest neighbor sites.  $\hat{c}_{i\sigma}^\dagger$  and  $\hat{c}_{j\sigma}$  are the creation and annihilation fermion operators. The fermion density is defined as usual as  $\hat{n}_i = \hat{n}_{i\uparrow} + \hat{n}_{i\downarrow}$  with  $\hat{n}_{i\sigma} = \hat{c}_{i\sigma}^\dagger \hat{c}_{i\sigma}$ . The first term in Eq. (1) represents the kinetic energy, where the hopping amplitude is taken to be time-dependent and by using the Peierls substitution becomes  $h_{ij}(t) = h_{ij}(0) e^{\frac{ie}{\hbar c} \phi(t)}$  with  $h_{ij}(0) = [h_0 + (-1)^i \eta]$ .  $\phi = \phi_{tot}/L$  is the total magnetic flux piercing the ring divided by the number of sites and  $\eta$  models a dimerization term. Hereafter we consider  $\hbar = e = a = 1$ , where  $a$  is lattice constant. Interactions are either local between fermions with opposite spins, described by  $U$ , or non-local between fermions sitting on neighboring sites, described by  $V_{ij}$ . All of the coupling constants which are reported in the following are scaled with  $h_0 = 1$ . Throughout this work

we consider an electric field, which is given by the time derivative of the flux,  $\tilde{F} = -\dot{\phi}(t)$ .

Starting from parameters at  $t = 0$  we find the ground state of the resulting Hamiltonian and propagate it while considering the change of the coupling parameters as function of time. To find the solution of the time-dependent Schrödinger equation,

$$H(\phi(t))|\psi(t)\rangle = i|\dot{\psi}(t)\rangle, \quad (2)$$

one may write it as a superposition of the instantaneous eigenstates of the time-dependent Hamiltonian as,

$$|\psi(t)\rangle = \sum_n c_n(t) |n_\phi(t)\rangle, \quad (3)$$

where  $|n_\phi(t)\rangle$  are the instantaneous eigenstates of  $H(\phi(t))$  with  $H(\phi(t))|n_\phi(t)\rangle = E_n(t)|n_\phi(t)\rangle$ . By substituting  $|\psi(t)\rangle$  as expressed by Eq. (3) into the Schrödinger equation and by using the change of variables as  $\tilde{c}_n(t) = c_n(t)e^{i\theta_{mn}(t)}$ , one obtains the following set of coupled differential equations for the coefficients  $\tilde{c}_n(t)$ ,

$$\dot{\tilde{c}}_n(t) = - \sum_{m \neq n} e^{i\theta_{mn}(t)} \tilde{c}_m(t) \langle n_\phi(t) | \dot{m}_\phi(t) \rangle, \quad (4)$$

where  $\theta_{nm}(t) = \int_0^t (E_n(\tau) - E_m(\tau)) d\tau - i \int_0^t (\langle n_\phi(\tau) | \dot{n}_\phi(\tau) \rangle - \langle m_\phi(\tau) | \dot{m}_\phi(\tau) \rangle) d\tau$ , this change of variables is in fact a gauge transformation because  $\theta_{nm}(t)$  are purely real<sup>40</sup>.

The change of basis set as function of time manifests itself in the  $\langle n_\phi(t) | \dot{m}_\phi(t) \rangle$  term in the right-hand side of Eq. (4). By starting from an eigenstate of the Hamiltonian at  $t = 0$  with  $|c_n(0)| = 1$ , as long as the terms  $\langle n_\phi(t) | \dot{m}_\phi(t) \rangle \simeq 0$  during the evolution, then one arrives at the adiabatic regime where  $|\psi(t)\rangle$  only follows the eigenstate of the instantaneous Hamiltonian and the coefficients  $|c_n(t)| = 1$  only consist of a phase that is a combination of a geometrical Berry and a dynamical phase. For the non adiabatic regime, Eq. (4) not only ensures the change in the magnitude of  $c_n(t)$  but each coefficient further accumulates a complicated phase consisting of dynamical and Berry phases produced by the other states.

If we consider the ground-state as the starting state for the time evolution, the quantity that measures the change of basis set as function of the external parameter  $\phi$  is the *ground-state fidelity*<sup>41</sup> which is defined as

$$\Xi(\phi) = |\langle \psi_0(\phi) | \psi_0(\phi + \delta\phi) \rangle|. \quad (5)$$

By using perturbative arguments it is possible to see that there is a close relationship between the ground-state fidelity and the coefficients that appear in Eq. (4),

$$\langle n(t) | \dot{m}(t) \rangle = \dot{\phi} \frac{\langle n_\phi(t) | \partial_\phi H(\phi(t)) | m_\phi(t) \rangle}{(E_n - E_m)}. \quad (6)$$

Therefore the change in the ground-state wave-function under an infinitesimal change of flux can be written as:

$$|\psi_0(\phi+\delta\phi)\rangle = \Lambda \left[ |\psi_0(\phi)\rangle + \delta\phi \sum_{n \neq 0} \frac{\langle n_\phi | \partial_\phi H(\phi) | \psi_0(\phi) \rangle}{E_0 - E_n} |n_\phi\rangle \right] \quad (7)$$

where  $\Lambda$  is a normalization factor. After normalization and considering  $\delta\phi \ll 1$  one obtains that

$$|\langle \psi_0(\phi) | \psi_0(\phi + \delta\phi) \rangle|^2 = 1 - (\delta\phi)^2 \chi_\Xi(\phi), \quad (8)$$

where  $\chi_\Xi(\phi)$  is the *fidelity susceptibility* which is defined as<sup>33,42</sup>,

$$\chi_\Xi(\phi) = \frac{1 - \Xi^2(\phi)}{(\delta\phi)^2} = \sum_{n \neq 0} \frac{\langle \psi_0(\phi) | \partial_\phi H(\phi) | n_\phi \rangle^2}{(E_0 - E_n)^2}. \quad (9)$$

The leading term in the fidelity expansion is of the order of  $\delta\phi^2$ . When comparing the terms in the right-hand side of Eq. (9) with terms that appear in the right-hand side of Eq. (4) one may infer that a larger  $\chi_\Xi(\phi)$  leads to a more non-adiabatic character of the transition due to the driving of the system by an external electric field. We will use the ground-state fidelity susceptibility in the following sections as a basis for the comparison of the short term response of different kinds of interacting fermions modeled by Eq. (1). We do this in particular when the system is subjected to a constant and uniform electric field.

Although the instantaneous eigenstate representation of the time-dependent Schrödinger equation is very insightful, the solution of Eqs. (4) is either very difficult or outright impossible for systems where the Hilbert space is very large and having the eigenstates at each moment is very computationally expensive. For the case of interacting fermions with spin the dimension of the Hilbert space for a small system which consists only 10 sites at half filling is  $\sim 63000$ , which makes solving Eqs. (4) almost impossible.

An alternate way to deal with the time-dependent Schrödinger equation is to exploit the form of the unitary time evolution operator:

$$\hat{U}(t) = \mathcal{T} e^{-i \int_0^t \hat{H}(\tau) d\tau} \simeq \prod_k e^{-i \hat{H}(t_k) \delta t}, \quad (10)$$

where  $\delta t = t_f/N$ . Therefore, the problem is reduced to a stepwise change of the Hamiltonian and relaxation of the system with a time step equal to  $\delta t$ . Over each time-step the Hamiltonian is considered to be time-independent and the relaxation of the wave function can be easily performed, by using the Chebyshev propagation method<sup>1</sup>, which considers an expansion of the evolution operator. The wave-function at  $t_i + \delta t$  can now be written as:

$$|\psi(t_k + \delta t)\rangle = e^{-ib\delta t} [J_0(a\delta t)I + \sum_{s=1}^{\infty} 2(-i)^s J_s(a\delta t) T_s(\tilde{H})] |\psi(t_k)\rangle, \quad (11)$$

where  $\tilde{H} = (\hat{H} - bI)/a$  with  $b = (E_{max} + E_{min})/2$  and  $a = (E_{max} - E_{min})/(2 - \epsilon)$ .  $J_s$  are  $s$ -th order Bessel functions of the first kind and  $T_s(x)$  are the Chebyshev polynomials which obey the recursion relation,  $T_s(x) = 2xT_{s-1}(x) - T_{s-2}(x)$ .  $\epsilon$  is introduced in order to make sure that the absolute value of the extreme eigenvalues of  $\tilde{H}$  is less than 1. This is crucial for the Chebyshev method because the arguments of Chebyshev polynomials accept only values in the interval  $[-1, 1]$ . We truncate the series in Eq. (11) such that the propagated wave function becomes normalized up to machine accuracy in order to reduce error accumulation during the stepwise propagations. Moreover this also ensures that the propagation operator is unitary up to machine accuracy. Having the wave function at each time-step, then the coefficients from Eq. (1),  $c_n(t) = \langle n_\phi(t) | \psi(t) \rangle$ , could be calculated for analysis purposes only whenever it is necessarily or possible to do so.

In order to have some insight about the nature of the wave-function,  $|\psi(t)\rangle$ , we further calculate the structure factors that are defined as,

$$C_X(q) = \frac{2}{L^2} \sum_{i=1}^L \sum_{j=1}^{L/2} e^{iqr_{i,i+j}} \bar{X}_{i,i+j} \quad (12)$$

where  $\bar{X}_{s,k} = \langle \hat{X}_s \hat{X}_k \rangle - \langle \hat{X}_s \rangle \langle \hat{X}_k \rangle$ ,  $s$  and  $k$  are the site indices (summation over  $L/2$  for  $j$  is introduced because  $\bar{X}_{s,k}$  is symmetric around  $\bar{X}_{s,s+L/2}$  due to the periodic boundary condition we considered) and  $r_{s,k}$  is the distance between site  $s$  and site  $k$ . We report spin density wave(SDW) order parameter  $O_{SDW} = C_{\hat{S}}(\pi)$  with  $\hat{S}_s = 1/2(\hat{n}_{s\sigma} - \hat{n}_{s\bar{\sigma}})$  and charge density wave(CDW) as  $O_{CDW} = C_{\hat{n}}(\pi)$ , where  $\hat{n}_s = \hat{n}_{s\sigma} + \hat{n}_{s\bar{\sigma}}$  is the local density operator. We also report the value of the current as function of time, which is defined as the expectation value of the current operator,  $\hat{J} = \frac{i}{L} \sum_{\langle sk \rangle \sigma} [h_{sk}(t) \hat{c}_{s\sigma}^\dagger \hat{c}_{k\sigma} - h.c.]$ .

### III. RESULTS

In the following we set  $h(0) = h_0 = 1$  and all the coupling constants are scaled with  $h_0$ . Moreover we define the uniform electric field,  $\tilde{F}$ , as  $\phi(t) = -\tilde{F}t$ . For the sake of simplicity we define  $F = \tilde{F}/2\pi$ . We consider the time steps to be  $\delta t = 0.005$ . We have tested all the results against a finer time grid in order to ensure that there is no quantitative difference over the parameter range considered here.

We start by showing in Fig. 1 the fidelity susceptibility,  $\chi_\Xi(\phi)$ , at  $\phi = 0.1\pi$  for a system consisting of 10 sites at half-filling for different values of  $U$  and as a function of  $V$ , we use  $\delta\phi = 10^{-3}$  for the calculations presented in Fig. 1. As is clear from the inset of Fig. 1,  $\chi_\Xi(\phi)$  acquires the largest value at  $\phi_{anti} = 0.1\pi$ , which is an anti-crossing point between the ground-state and an excited state. Notice that here we calculate  $\chi_\Xi(\phi)$  numerically exact with the use of the Lanczos method and do not use the perturbative form introduced in Eq. (9).

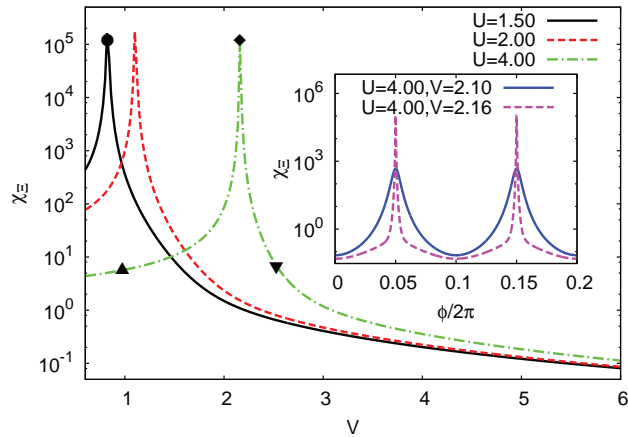


FIG. 1. (Color online) Fidelity susceptibility for a ring with  $L_{sites} = 10$  and  $N_{\uparrow} = N_{\downarrow} = 5$  at  $\phi = 0.1\pi$  as function of interactions. The inset shows the fidelity susceptibility as function of  $\phi/2\pi$  for different sets of parameters. The points represent specifically chosen pairs of parameters  $U, V$  in order to model a weakly interacting metal (circle), a SDW insulator (triangle), a CDW insulator (upside down triangle) and a strongly interacting metal (diamond).

Notice that the susceptibility is largest, almost diverging, at specific values of  $V$  for each  $U$ , whenever the relation  $U \simeq 2V$  is satisfied. This relation represents the boundary which separates the SDW and CDW phases<sup>43</sup>, and was obtained within the DMRG approach for 1D chains of larger dimensions. However, it is obvious that  $\chi_{E}(\phi_{anti})$  can provide a good estimate on the location of the SDW-CDW phase boundary, although it does not provide any information about the details of the wavefunction (whether it describes SDW or CDW).

In order to compare the non-linear response of different kinds of interacting systems we analyze different sets of interaction and hopping parameters. In particular we study three different cases: first we consider a system with  $U = 1.5$  and  $V = 0.82$ , marked with a circle in Fig. 1, which shows an almost diverging  $\chi_{E}(\phi_{anti})$  and has a vanishingly small charge gap,  $\Delta_{charge}(\phi_{anti}) \simeq 10^{-3}$ , and therefore could be considered as a *weakly interacting metal*. Secondly, we use a dimerization parameter  $\eta = 0.4$ , which opens up a gap and the system behaves as a *correlated band insulator* (BI). Finally, we choose a stronger interacting system with  $U = 4.0$  and three different values of  $V = 0.94, 2.56$  and  $1.16$ . Two values,  $V = 0.94$  (a *SDW insulator*, marked with a triangle in Fig. 1,  $\Delta_{charge}(\phi_{anti}) = 1.44$ ) and  $V = 2.56$  (a *CDW insulator*, marked with an upside down triangle in Fig. 1,  $\Delta_{charge}(\phi_{anti}) = 1.36$ ) are chosen such that  $\chi_{E}(\phi_{anti})$  is the same. We also consider  $V = 1.16$  on the phase boundary between SDW and CDW with an almost diverging  $\chi_{E}(\phi_{anti})$  (marked with a diamond in Fig. 1). The latter case also has a vanishingly small charge gap but it should be considered as a *strongly interacting metal*.

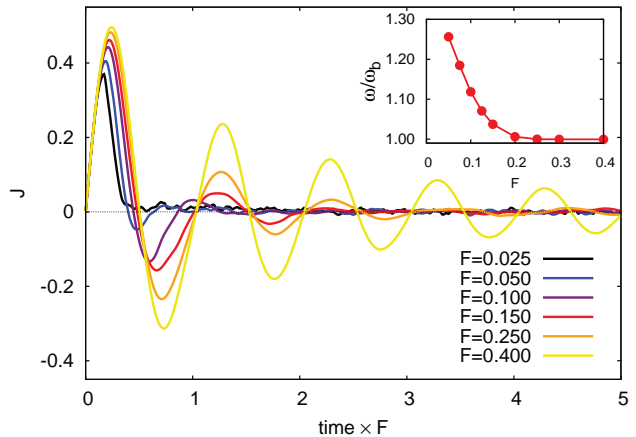


FIG. 2. (Color online) Current as function of time for a ring with  $U = 1.5$ ,  $V = 0.82$ ,  $L_{sites} = 10$ ,  $N_{\uparrow} = N_{\downarrow} = 5$  and for different electric field strengths. Inset: the frequency of the BO for different electric fields and the same parameters of the main graph with  $\omega_b = F$ .

### A. Weakly interacting system

In Fig. 2 we show the current as function of time for a system with  $U = 1.5$  and  $V = 0.82$  for different electric field strengths. For illustrative purposes we start the analysis of the graph from the largest field,  $F = 0.4$ , where it shows a regular damped BO in the time domain of interest. As we stated previously,  $\chi_{E}(\phi_{anti})$  is largest at the anti-crossings, thus the probability transfer from the ground-state to excited states (also in analogy with LZ theory) is enhanced. Therefore at each anti-crossing there is a high probability of transfer from a right going wave ( $-\partial E_n(\phi)/\partial\phi > 0$ ) to another right going wave. When the field is strong enough this transfer is very efficient such that the wave-function has a significant overlap with *only one* of the eigenstates of the instantaneous Hamiltonian. Finally when the maximum energy is reached, the wave-function will start having significant overlap with left-going states and the current will change sign. This reflection for the high field case happens exactly at  $t = (2F)^{-1}$ .

To better understand the above description of the large field response, we plot in Fig. 3(a) the eigenstates of the instantaneous Hamiltonian as a function of time for a smaller system, with  $L = 6$  at half-filling, for  $F = 0.4$  and the same interaction parameters. Both the size of the points and their color code represent the magnitude of the overlap of the time-dependent wave-function with the instantaneous eigenstates of  $\hat{H}(t)$ . Note that the spectrum is periodic with  $2\pi/L$ , thus the first anti-crossing happens at  $tF = 0.5/L = 0.833$ . This smaller ring shows very similar behavior to the one presented in Fig. 2 when subjected to a strong field, except that the magnitude of the current is smaller. The formation of a coherent path for the probability transfer throughout the spectrum and the reflection at the topmost state when  $t = (2F)^{-1}$  can

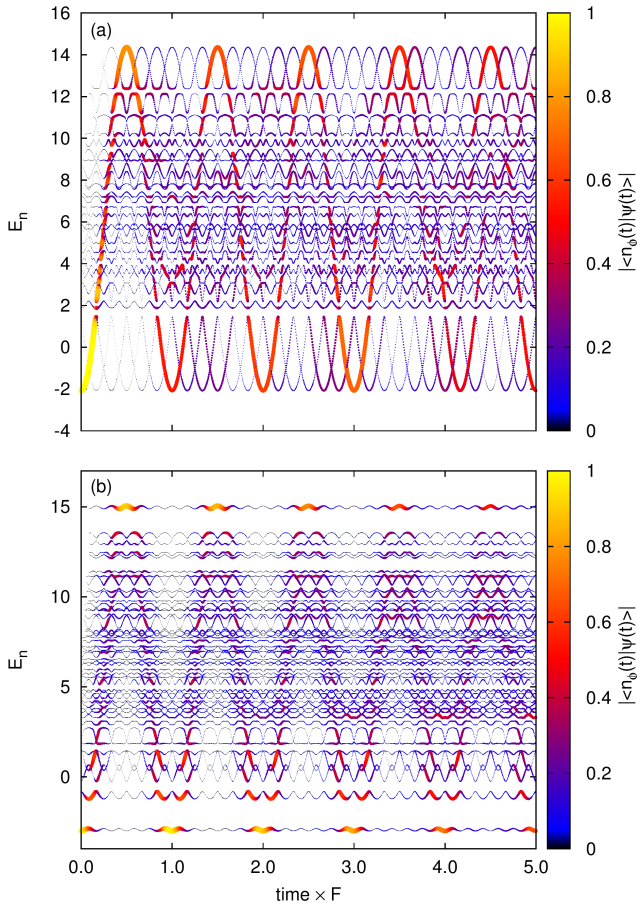


FIG. 3. (Color online) (a) Eigenvalues of the instantaneous Hamiltonian as function of time for a system with  $L=6$  at half filling,  $U=1.5, V=0.82, F=0.4$ . The colors and the size of the points are given by the overlap of the time-dependent wave-function with the instantaneous eigenstates,  $|\langle n_\phi(t)|\psi(t)\rangle|$ ; (b) The same as (a) but with a dimerization parameter  $\eta = 0.4$  and  $F=4.0$ .

be clearly seen. However, a dissipative loss of the probability to both left-going and right-going waves is possible and the current becomes damped as function of time. For higher fields the probability transfer is more efficient, which means that the damping of BO is suppressed.

*Weak fields.* Looking back to Fig. 2, the weakest field response, for  $F = 0.025$ , is comprised of two non-linear effects. First, the state with high probability is reflected sooner, well before it arrives at the other edge of the spectrum. This could be inferred from the fact that the current changes sign sooner than in the high field case. Second, when the field is weak the probability transfer to excited states is smaller, which means that at each higher energy anti-crossing there is a finite probability of remaining in the state with lower energy, which will contribute with a negative sign to the total current. Therefore after an initial increase in current, the wave-function will overlap with equally right-going and left-going instantaneous states and one ends up with a quasi-

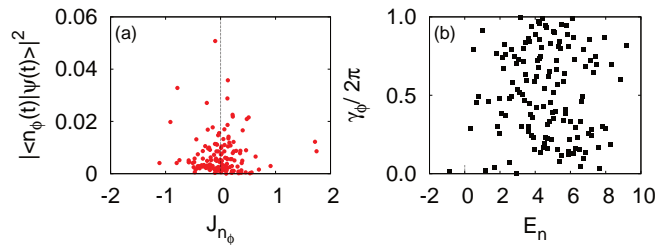


FIG. 4. (Color online) (a)  $|\langle n_\phi(t)|\psi(t)\rangle|^2$  for  $L_{sites} = 8$  and  $N_\uparrow = N_\downarrow = 4, U = 1.5, V = 0.82$  and  $F=0.025$  at  $tF = 2.51$ ,  $|n_\phi(t)\rangle$  are the eigenstates of instantaneous Hamiltonian; (b)  $\gamma_n = \arg(\langle n_\phi(t)|\psi(t)\rangle)$  for the same parameters.

stationary regime in which the current is very small and fluctuates around zero.

We further elucidate this behavior by expressing the current as function of instantaneous eigenstates of  $\hat{H}(t)$ ,

$$\langle \hat{J} \rangle = \sum_n c_n(t)^2 \langle n | \hat{J} | n \rangle + \sum_{n \neq m} c_n(t) c_m(t) e^{i(\gamma_n - \gamma_m)} \langle m | \hat{J} | n \rangle \quad (13)$$

where  $c_n(t) = |\langle n_\phi(t)|\psi(t)\rangle|$  describes the magnitude of the overlaps of the time-dependent wave-function with the instantaneous eigenstates and  $\gamma_n = \arg(\langle n_\phi(t)|\psi(t)\rangle)$  describe the phases acquired by the wave-function.

We plot in Fig. 4(a), for  $F = 0.025$  and  $L = 8$ ,  $c_n(t)$  as function of the current for each eigenstate at time  $tF = 2.51$ . Observe that the probability amplitudes as function of current are approximately symmetrically distributed between left-going and right-going states, this in turn implies that the first term of Eq. (13), i.e. the diagonal expectation value of the current, becomes approximately equal to 0. Moreover, the phases,  $\gamma_n$ , which are presented in Fig. 4(b) are distributed uniformly between 0 and  $2\pi$  therefore leading to the dephasing of non-diagonal terms in Eq. (13), and finally the total current is approximately equal to zero. One should notice that for the case with  $L = 8$  the current is not completely equal to zero, but it acquires a small but finite value that fluctuates around zero, indicating the fact that the number of eigenstates that contribute is small due to finite size effects. These fluctuations are suppressed for larger systems as we show in the following sections.

*Intermediate fields.* We next analyze the response to intermediate fields between the full dissipative case for  $F = 0.025$  and the full oscillating one for  $F = 0.4$ . When the electric field strength is increased the reflection of the high probability state gradually approaches the largest eigenstate of the spectrum. This could be clearly recognized in Fig. 2 where the time,  $tF$ , for which the current changes its sign approaches 0.5. At the same time the BO period, which is generally less than  $F^{-1}$ , gradually approaches  $F^{-1}$ . This is shown in the inset of Fig. 2 where we plot the frequency of BO as function of field strength. A similar behavior was also reported in metallic spin-less systems subjected to an uniform electric field<sup>38</sup>. Our investigation should also be relevant to

that case. Similar to the electric breakdown case, where a mapping to a quantum random walk<sup>44</sup> on a semi-infinite chain was proposed, here the problem of BO damping also could be mapped to a quantum random walk but on a chain with two edge states. However, as we will present in the following, the actual long time response to an electric field depends strongly on the probability transfer between subsequent states throughout the whole spectrum. It is therefore necessary to design a random walk for which the probability transfer is also randomized but taken from specific distributions, which could be chosen based on the level statistics of the Hamiltonian<sup>45</sup>.

*Dimerization.* In Fig. 5, we show the current as function of time for a system with the same interactions as in the metallic case but with a dimerization parameter  $\eta = 0.4$ . We call this state a correlated band insulator(BI). The general also arguments presented for the metallic case hold here, however there are also differences, which we explain in the following. As expected, dimerization induces the opening of a charge gap ( $\Delta_{charge}(\phi_{anti}) = 1.74$ ) and the electric field breakdown is postponed to larger fields. Additionally, a dissipative regime appears only at  $F = 0.2$ . At this field strength the breakdown has already happened and the instantaneous ground state has a very small contribution to  $|\psi(t)\rangle$ . For larger fields, i.e.  $F = 0.4$ , first the current starts to show irregular oscillations, then at  $F = 0.6$  the current becomes oscillatory but with a frequency of the BO larger than  $F$ . Finally, at even larger fields,  $F = 4.0$ , the current is oscillatory with  $\omega = F$ . This is achieved for much larger fields than the ones presented for the weakly interacting metal, as shown in the inset of Fig. 5. The first notable difference between the metal and the correlated BI is that here BOs with smaller frequencies survive for longer times. This is different from the metallic case where BOs with smaller frequencies are strongly damped. Furthermore, one may expect that the dimerization may only postpone the breakdown and the transition to the oscillatory behavior should not be affected as long as the dimerization only affects the low energy part of the spectrum by opening up a ground-state charge gap. However, the presence of long lasting BO with the period less than  $F^{-1}$  implies the presence of states with small  $\chi_{\Xi}$  in the middle of the spectrum and which reflects a high probability state back. Roughly speaking, these states could be at the edge of a cluster of eigenstates, and are separated by a large gap from the next subsequent state and therefore play the rule of an edge state. However, we emphasize that not only the gap but also the actual value of  $\chi_{\Xi}$  of each eigenstate are important factor that affect the non-adiabatic behavior of the system. In order to visualize again the overlap of the time-dependent wave-function with the whole spectrum, we turn back to Fig. 3(b), where the overlap with the instantaneous eigenstates of  $\hat{H}(t)$  is plotted as function of time for a smaller dimerized system with  $L = 6$ ,  $\eta = 0.4$  and  $F = 2.0$ . Again the smaller ring behaves the same as a larger system with  $L = 10$  when subjected to

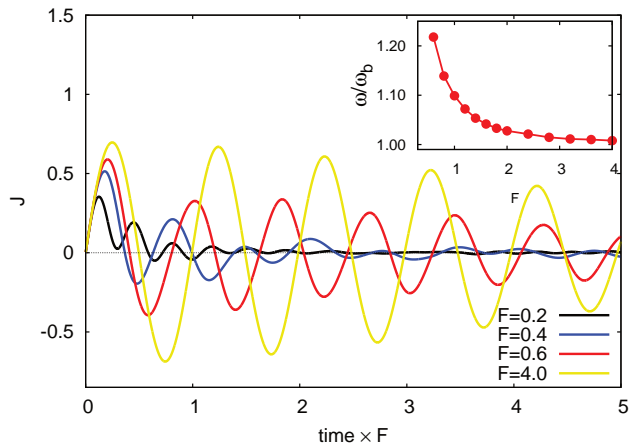


FIG. 5. (Color online) Current as function of time for a dimerized ring with  $L_{sites} = 10$  and  $N_{\uparrow} = N_{\downarrow} = 5$ ,  $U = 1.5$ ,  $V = 0.82$ ,  $\eta = 0.4$  (see the definition of the hopping parameter following Eq. 1) and for different electric field strengths. The inset shows the frequency of the Bloch oscillations for different electric fields and the same parameters of the main graph with  $\omega_b = F$ .

strong fields. As is clear from the plot the recurrences of the ground-state and the state with largest energy occur periodically at  $F^{-1}$ . A noticeable feature of the propagation in the dimerized systems is the fact that the overlap of  $|\psi(t)\rangle$  with the instantaneous eigenstates is very non-local in the energy domain, meaning that the path of high probability transition is broadened in comparison to the metallic system. Noticeably, the wave-function starts to have finite overlap around the first anti-crossing not only to the first excited state but also with the second excited state. Therefore, a two level approximation (LZ-like) is not appropriate for the ground-state breakdown. The dimerization leads to a stronger insulator not only in the sense that it postpones the electric field breakdown, but it also largely affects the overlap with states located in the middle of the spectrum. In short, while the breakdown and the appearance of the dissipative behavior mostly depends on the low energy part of the spectrum, the transition from the dissipative to the oscillatory behavior largely depends on the clustering of eigenstates in the middle of the spectrum.

## B. Strongly interacting system

For the cases with strong interactions, as stated before, we choose  $U = 4.0$  and three different nearest neighbor interactions,  $V = 0.94$  (SDW insulator),  $V = 2.56$  (CDW insulator) and  $V = 2.16$  (metallic case). For the insulating cases we choose the interaction parameters such that both cases acquire the same ground state  $\chi_{\Xi}(\phi_{anti})$  as seen in Fig. 2. We plot, in Fig. 6(a), the current as function of time for a very small electric field, i.e.  $F = 0.002$ , for a ring of size  $L = 10$ . Both insulating systems appear

to be in the adiabatic regime, where the current shows an oscillatory behavior with a period equal to  $F/L$ . However, the metallic case shows oscillations with a doubled period,  $2F/L$ . The main reason for this comes from the fact that for the metallic case the probability is transferred completely to the first excited state due to very large  $\chi_{\Xi}(\phi_{anti})$ , i.e. it cannot be considered in the adiabatic regime even at these small fields. This is illustrated in Fig. 6(b), where the energies of the first three states of the  $\hat{H}(t)$  are shown as function of time (and implicitly as a function of flux), together with the overlap of  $|\psi(t)\rangle$  to these three states. As is obvious, because of the very large  $\chi_{\Xi}$ , there is a very large overlap to the first excited state after the first anti-crossing, however the field is very small such that it cannot overcome the gap between the first excited and second excited state.  $|\psi(t)\rangle$  only has an extremely small overlap with second excited state, which leads to the fact that the probability is reflected back to the ground state and one ends up with current oscillations with a period twice of the adiabatic expectation. The breakdown field is now achieved when the gap between the first and second excited states is overcome. We next describe the response of strongly interacting systems to larger fields. In Fig. 6 we present the current as function of time for different field strengths and for the three interaction choices introduced previously. For  $F = 0.1$  all the cases shows a dissipative behavior, however the insulating ones show small peaks in the current before it arrives at the quasi-stationary zero-current state. The period of these peaks is approximately equal to  $F/L$ , which therefore implies that the overlap of  $|\psi(t)\rangle$  with the instantaneous ground state does not vanish quickly and manifest itself as small peaks in the current. This is not the case for  $V = 2.16$  where the overlap with the ground state is lost immediately at the anti-crossing (see the inset of Fig. 6 for  $F = 0.2$ ) and the current behaves smoothly from the beginning of the evolution. For stronger fields,  $F = 0.2$ , the change of the current is large, such that the current fluctuations due to the finite overlap with the ground-state disappear. In the inset of Fig. 6 we show the square of the overlap of  $|\psi(t)\rangle$  with the ground-state of the instantaneous Hamiltonian. It is clear that for the two insulating cases for which we set  $\chi_{\Xi}(\phi_{anti})$  to be equal, the decay of the ground-state is identical. Furthermore, in the dissipative cases for  $F = 0.1$  and  $F = 0.2$  both insulating cases behave almost in the same way even for larger times even though the interaction strengths are very different and one describes an SDW insulator while the other one an CDW insulator with different excitation. This means that by setting  $\chi_{\Xi}(\phi_{anti})$  the same, not only the ground-state decay is identical but also the tunneling to the lower part of spectrum the behaves very similarly. When the field is increased to  $F = 0.8$ , the SDW insulator with  $V = 0.94$  starts to show Bloch-like oscillations with large amplitude. On the other hand the metallic and CDW cases are still in the dissipative regime with a vanishingly small long-time current. For even larger fields,  $F \simeq 1.6$  (not shown here), all three cases show

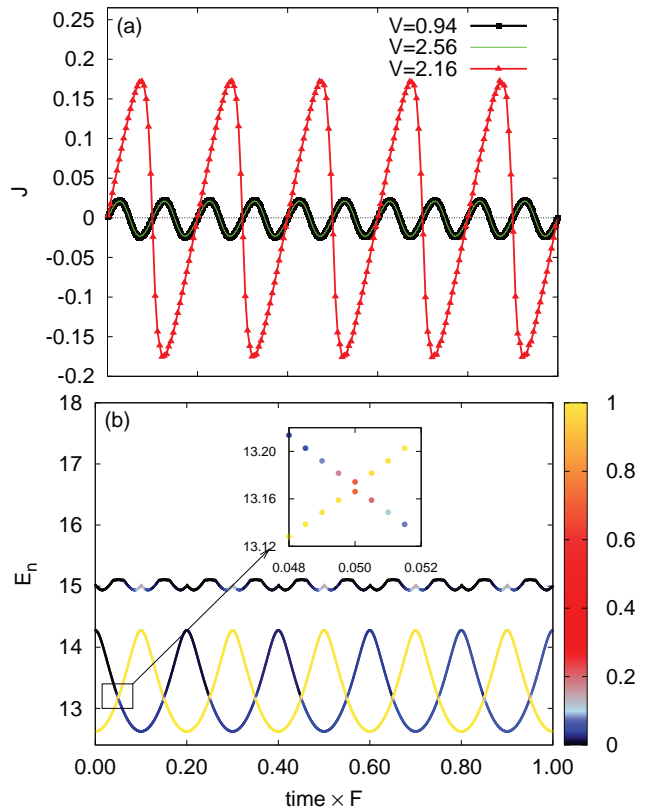


FIG. 6. (Color online) (a) Current as function of time for very small field  $F = 0.002$  for different interactions; (b) The energy dispersion of the first three excited states of instantaneous Hamiltonian together with the square of these states with  $|\psi(t)\rangle$  as function of time for  $U=4.0, V=1.16$ . The inset of panel (b) shows a zoom-in into the anti-crossing region. Colors represent the overlap of the time-dependent wave-function with the instantaneous eigenstates.

oscillations with large amplitude but which are irregular. It is only when the strength of the electric field is very large,  $F = 10.0$ , that all the cases show regular BO oscillations as shown in Fig. 6.

*Finite size effect.* To see the effect of the size of the system on the transition from a dissipative to an oscillatory pattern, we plot in Fig. 8 the current as function of time for different sizes for  $V = 0.94$  (SDW insulator) and  $V = 2.56$  (CDW insulator). We observe that for all cases the fluctuations of the current in the dissipative regime ( $F = 0.2$ ) are suppressed for larger sizes. This is due to the fact that  $|\psi(t)\rangle$  acquires overlap with a much larger number of states when the size is increased. This implies that a more efficient dephasing of the current is achieved (see the discussion following Eq. 13). However, in the strong-field regime, once the transition to oscillatory behavior occurs, the size effect is negligible, showing that the sizes of the gaps in the middle of the spectrum do not depend strongly on the size, at least not for the strong interactions considered here.

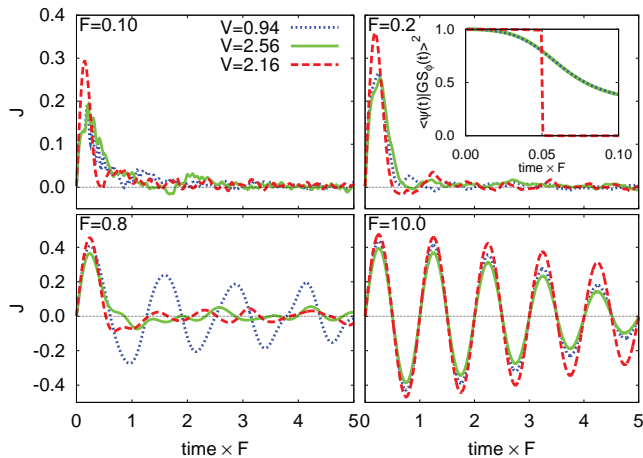


FIG. 7. (Color online) Current as function of time for different interactions and different field strength. The inset shows the square of the overlap of  $|\psi(t)\rangle$  with the instantaneous ground state of  $H(t)$  for different interactions and  $F = 2.0$ .

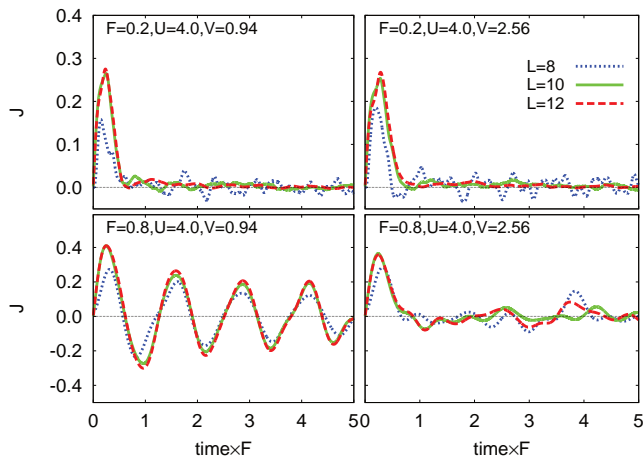


FIG. 8. (Color online) Current as function of time for different interactions and different field strengths and different sizes.

*Order parameters.* In Fig. 9, we show the SDW and CDW order parameters as function of time for the two insulating cases. As is clear from Fig. 9(b) for the SDW ordered system,  $O_{SDW}$  only drops gradually as function of time, however at the same time  $O_{CDW}$  is enhanced at the beginning of the evolution. This further implies the presence of a CDW state near the bottom of the spectrum<sup>46</sup>. Finally at longer times both order parameters dissipates during the evolution arriving at a quasi-stationary state with almost vanishing value for larger times. The CDW ordered system shows a similar behavior but with reversed  $O_{CDW}$  and  $O_{SDW}$  contributions (see Fig. 9(b)). Therefore, the transient regime shows that since the two order parameters are in competition, the mechanism of destroying the dominant order is the proliferation of the competing one.

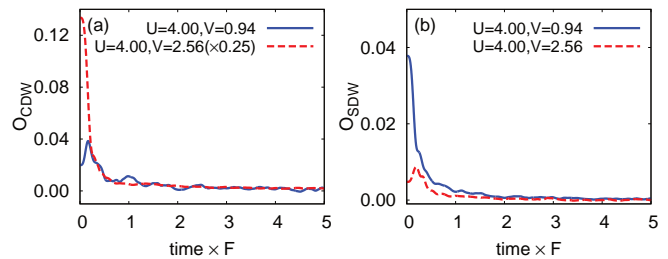


FIG. 9. (Color online) (a) CDW order parameter as function of time for a system with  $L=12$  at half filling derived with  $F = 0.2$ ; (b) SDW order parameter as function of time and the same parameters as in plot(a).

#### IV. CONCLUSIONS

In conclusion we investigated the nonlinear response of a closed interacting fermionic system as modeled by an extended Hubbard model. Weakly interacting metallic system at the boundary of SDW-CDW, shows a dissipative behavior for low fields. The main reason for this is the fact that  $|\psi(t)\rangle$  acquires overlap with large number of left going and right going states. This in turn implies that the quasi-stationary state acquires zero current. Bloch oscillations start smoothly with a frequency larger than  $F$ . The main reason for this is the fact that the reflection happens at the lower part of the spectrum, thus effectively decreasing the bandwidth. Upon increasing the field strength the probability transfer at each anti-crossing is more efficient. This leads to a more regular recurrences of the ground state and the topmost excited state with period of  $F^{-1}$ , which can be seen from the oscillations in the current. Upon dimerization of the metallic system, the formation of the dissipative regime is postponed to larger fields due to the formation of a charge gap. However, the main difference between the dimer case and the metallic system resides in the fact that, first, it shows irregular current oscillations before they turn into regular BO and second, the BO with larger frequencies survive for large times, in analogy with the metallic case subjected to strong field. This implies the existence of states at the middle of the spectrum with low  $\chi_{\Xi}(\phi)$  (or roughly speaking the formation of large mid gaps in the relevant excitations) that play the role of a band-edge state and reflect back the overlap probability at the middle part of the spectrum even for large electric fields. Finally, the dimerized system also shows regular BO with period equal to  $F^{-1}$  for large enough electric fields. The value for which the dimerized system shows regular BO are much larger than those found for the metallic system even though the interactions are identical.

For stronger interacting systems when the interactions are chosen such that the ground-state  $\chi_{\Xi}(\phi_{anti})$  is the same for both cases, then the ground state decay for both CDW insulator and SDW insulator behaves exactly the same. This similarity of the ground-state decay mani-



fects itself even for larger times and for both low and high field dissipative regimes. However significant differences arise between the two cases for large electric fields. While SDW shows oscillatory behavior with large magnitude the CDW insulator and strong interacting metallic system only shows irregularities with small oscillations. Different from the weakly interacting metallic system and the dimer case, in the strongly interacting regime these irregularities are extended to intermediate fields and only for very large fields,  $F = 10.0$ , regular BO with a period of  $F^{-1}$  are observed. This effect appears to be little affected by size, since the SDW and CDW insulators, for  $L=10$  and  $L=12$ , show the same qualitatively and even

quantitatively behavior. This implies that the reorganization of the spectrum is affected much more by the interaction than by the finite size induced discreteness.

## ACKNOWLEDGMENTS

This work was supported by the Flemish Science Foundation (FWO-VI) and Methusalem program of the Flemish government. One of us (LC) is a postdoctoral fellow of the FWO-VI.

\* [Davoud.NasrEsfahani@uantwerpen.be](mailto:Davoud.NasrEsfahani@uantwerpen.be)

† [lucian@covaci.org](mailto:lucian@covaci.org)

‡ [Francois.Peeters@uantwerpen.be](mailto:Francois.Peeters@uantwerpen.be)

- <sup>1</sup> A. Polkovnikov, K. Sengupta, A. Silva, and M. Vengalattore, *Rev. Mod. Phys.* **83**, 863 (2011).
- <sup>2</sup> A. Weiße, G. Wellein, A. Alvermann, and H. Fehske, *Rev. Mod. Phys.* **78**, 275 (2006).
- <sup>3</sup> M. Hochbruck and C. Lubich, *SIAM Journal on Numerical Analysis* **34**, 1911 (1997).
- <sup>4</sup> F. Verstraete, J. J. Garcia-Ripoll, and J. I. Cirac, *Phys. Rev. Lett.* **93**, 207204 (2004).
- <sup>5</sup> J. K. Freericks, *Phys. Rev. B* **77**, 075109 (2008).
- <sup>6</sup> M. Eckstein and P. Werner, *Phys. Rev. B* **88**, 075135 (2013).
- <sup>7</sup> F. Sawano, I. Terasaki, H. Mori, T. Mori, M. Watanabe, N. Ikeda, Y. Nogami, and Y. Noda, *Nature* **437**, 522 (2005).
- <sup>8</sup> Y. Taguchi, T. Matsumoto, and Y. Tokura, *Phys. Rev. B* **62**, 7015 (2000).
- <sup>9</sup> S. Iwai, M. Ono, A. Maeda, H. Matsuzaki, H. Kishida, H. Okamoto, and Y. Tokura, *Phys. Rev. Lett.* **91**, 057401 (2003).
- <sup>10</sup> H. Okamoto, H. Matsuzaki, T. Wakabayashi, Y. Takahashi, and T. Hasegawa, *Phys. Rev. Lett.* **98**, 037401 (2007).
- <sup>11</sup> M. Greiner, O. Mandel, T. W. Hansch, and I. Bloch, *Nature* **419**, 51 (2002).
- <sup>12</sup> M. Köhl, H. Moritz, T. Stöferle, K. Günter, and T. Esslinger, *Phys. Rev. Lett.* **94**, 080403 (2005).
- <sup>13</sup> I. Bloch, *Nat Phys* **1**, 23 (2005).
- <sup>14</sup> T. Esslinger, *Annual Review of Condensed Matter Physics* **1**, 129 (2010).
- <sup>15</sup> M. Eckstein, M. Kollar, and P. Werner, *Phys. Rev. B* **81**, 115131 (2010).
- <sup>16</sup> M. Eckstein, A. Hackl, S. Kehrein, M. Kollar, M. Moeckel, P. Werner, and F. A. Wolf, *Eur. Phys. J. Spec. Top.* **180**, 217 (2009).
- <sup>17</sup> C. Kollath, A. M. Lauchli, and E. Altman, *Phys. Rev. Lett.* **98**, 180601 (2007).
- <sup>18</sup> S. Genway, A. F. Ho, and D. K. K. Lee, *Phys. Rev. A* **86**, 023609 (2012).
- <sup>19</sup> M. Rigol and L. F. Santos, *Phys. Rev. A* **82**, 011604 (2010).
- <sup>20</sup> K. A. Al-Hassanieh, F. A. Reboredo, A. E. Feiguin, I. Gonzalez, and E. Dagotto, *Phys. Rev. Lett.* **100**, 166403 (2008).

- <sup>21</sup> M. Mierzejewski, J. Bonča, and P. Prelovšek, *Phys. Rev. Lett.* **107**, 126601 (2011).
- <sup>22</sup> M. Mierzejewski, L. Vidmar, J. Bonča, and P. Prelovšek, *Phys. Rev. Lett.* **106**, 196401 (2011).
- <sup>23</sup> M. Eckstein and P. Werner, *Phys. Rev. Lett.* **107**, 186406 (2011).
- <sup>24</sup> M. Eckstein, T. Oka, and P. Werner, *Phys. Rev. Lett.* **105**, 146404 (2010).
- <sup>25</sup> H. Lu, S. Sota, H. Matsueda, J. Bonča, and T. Tohyama, *Phys. Rev. Lett.* **109**, 197401 (2012).
- <sup>26</sup> A. Takahashi, H. Itoh, and M. Aihara, *Phys. Rev. B* **77**, 205105 (2008).
- <sup>27</sup> M. Mierzejewski, J. Luczka, and J. Dajka, *J. Phys.: Condens. Matter* **22**, 245301 (2010).
- <sup>28</sup> T. Oka, R. Arita, and H. Aoki, *Phys. Rev. Lett.* **91**, 066406 (2003).
- <sup>29</sup> T. Oka and H. Aoki, *Phys. Rev. Lett.* **95**, 137601 (2005).
- <sup>30</sup> L. D. Landau, *Phys. Z. Owjetunion* **2**, 46 (1932).
- <sup>31</sup> C. Zener, *Proc R. Soc. A* **137**, 696 (1932).
- <sup>32</sup> Z. Lenarčič and P. Prelovšek, *Phys. Rev. Lett.* **108**, 196401 (2012).
- <sup>33</sup> W.-L. You, Y.-W. Li, and S.-J. Gu, *Phys. Rev. E* **76**, 022101 (2007).
- <sup>34</sup> J. Feldmann, K. Leo, J. Shah, D. A. B. Miller, J. E. Cunningham, T. Meier, G. von Plessen, A. Schulze, P. Thomas, and S. Schmitt-Rink, *Phys. Rev. B* **46**, 7252 (1992).
- <sup>35</sup> K. Leo, P. H. Bolivar, F. Bruggemann, R. Schwedler, and K. Kohler, *Solid State Communications* **84**, 943 (1992).
- <sup>36</sup> C. Waschke, H. G. Roskos, R. Schwedler, K. Leo, H. Kurz, and K. Kohler, *Phys. Rev. Lett.* **70**, 3319 (1993).
- <sup>37</sup> P. Voisin, J. Bleuse, C. Bouche, S. Gaillard, C. Alibert, and A. Regreny, *Phys. Rev. Lett.* **61**, 1639 (1988).
- <sup>38</sup> M. Mierzejewski and P. Prelovšek, *Phys. Rev. Lett.* **105**, 186405 (2010).
- <sup>39</sup> L. Vidmar, J. Bonča, M. Mierzejewski, P. Prelovšek, and S. A. Trugman, *Phys. Rev. B* **83**, 134301 (2011).
- <sup>40</sup> M. Tomka, A. Polkovnikov, and V. Gritsev, *Phys. Rev. Lett.* **108**, 080404 (2012).
- <sup>41</sup> P. Zanardi and N. Paunković, *Phys. Rev. E* **74**, 031123 (2006).
- <sup>42</sup> S. Greschner, A. K. Kolezhuk, and T. Vekua, *Phys. Rev. B* **88**, 195101 (2013).
- <sup>43</sup> S. Ejima and S. Nishimoto, *Phys. Rev. Lett.* **99**, 216403 (2007).
- <sup>44</sup> T. Oka, N. Konno, R. Arita, and H. Aoki, *Phys. Rev. Lett.*

- [94, 100602 \(2005\)](#).
- <sup>45</sup> D. Poilblanc, T. Ziman, J. Bellissard, F. Mila, and G. Montambaux, [Euro. Phys. Lett.](#) **22**, 537 (1993).
- <sup>46</sup> H. Lu, S. Sota, H. Matsueda, J. Bonča, and T. Tohyama, [Phys. Rev. Lett.](#) **109**, 197401 (2012).